Changing patterns of thermal behaviour of concrete pavements in diurnal periods

Civil Engineering student report: Yuhan Mao

September 19, 2022

Supervisor: M.M. Rutten and E. Stache

Abstract

Concrete is affected by a variety of environmental factors, and its temperature varies with time and other meteorological factors. The subsequent construction of the Heat Square is supported by an analysis of concrete temperature changes and their environmental influences. This article evaluates the variation of concrete block temperature by two months of field measurements at the Heat Square and meteorological data from The Green Village. The temperature of the concrete bricks changed asymmetrically, with the cooling time being much longer than the warming time. The maximum temperature occurred in the early morning after sunset, with a 3-hour time delay between changes in concrete temperature. By using partial correlation analysis, the most significant influence of meteorological factors on the surface temperature was the air temperature and the least influence of changes in relative humidity on the surface temperature. The article's analysis offers two suggestions for the Heat Square's construction: (1) Include measurements of near-surface wind speed. (2) Combine temperature measurements taken at various depths. (3) Subsequent research can explore the cooling effect by analyzing the shading effect of plants.

Contents

1 Introduction

Buildings and concrete pavements have gradually occupied the surface of urban cities. Surface temperature and humidity regulation are lacking in cities, and these insulating materials alter the thermal behavior of the cities, resulting in a steady rise in ground and air temperatures with all the negative consequences that involves(Wonorahardjo et al., 2022). Over the past several decades, research efforts have been devoted to developing and evaluating various UHI mitigation strategies through measurements, remote sensing techniques, and numerical simulations. In the Netherlands, the likelihood of a severe summer heat island effect increasing in urban areas where the average summer midnight temperature is 4 to 8 °C higher than in the surrounding area, and the temperature variation has been increasing in recent years, which makes the city far less habitable(Hove et al., 2014). In contrast to the obvious drop in temperature in rural areas in the evening or after sunset, it is the cities where the pavements or buildings continue to radiate heat, maintaining a high temperature.

Previous research has addressed and analyzed the performance of certain thermal parameters, such as solar reflectance, thermal emissivity, conductivity, and capacity. These thermal parameters were discovered to be crucial for assessing various pavement strategies for UHI mitigation(Aletba et al., 2021). Pavement materials commonly applied in urban areas, such as concrete and asphalt mixes, have a relatively high solar energy absorption capacity as well as a high heat storage capacity, allowing them to retain large amounts of heat during the day and release it back into the air at night(Doulos, Santamouris, & Livada, 2004). During the day, asphalt roads and roofs in Tel-Aviv were the warmest regions in the research area, with external walls and trees having the greatest surface temperatures during the night(Chudnovsky, Ben-Dor, & Saaroni, 2004). Some researchers studied the warming effects of various pavement materials and the diurnal temperature fluctuations of vegetation and water surfaces by measuring the temperature changes of different pavements in cities during the day and night(Yang & Zhao, 2016). The cooling effect of reflective, permeable, and some innovative pavements has been extensively evaluated based on lab experiments, field experiments, and numerical simulations(Anupam, Sahoo, & Rath, 2020). However, the quantified general relationships between pavement properties (e.g., reflectance) and temperature changes at different spatial scales involve large uncertainties, as induced by a variety of factors such as background climate and weather conditions(Wang, Wang, Kaloush, & Shacat, 2021). In addition, the relationship between reflectance and human thermal comfort is usually assessed via numerical simulations, while realistic field-based observations are relatively rare(Middel, Turner, Schneider, Zhang, & Stiller, 2020). As for in-field measurements, some research has used computer simulations to evaluate temperature variations under local climate conditions(Engineering ToolBox, 2003). The previous research also includes urban landscaping and building structures for the analysis of local urban climate change patterns and vegetation performs the best overall in UHI mitigation potential.(Stache, Schilperoort, Ottelé, & Jonkers, 2022).

The thermodynamic properties of cities have a significant impact on their local climate, and the effects of their heat absorption and release patterns, as well as interactions with meteorological parameters, on the urban heat island effect still need to be studied.

2 Materials and Method

2.1 Study Area

The measurements were performed in the Green Village on the Delft University of Technology campus, which is located in the heat square at 51.99 N, 4.37 E. The square(Figure 5) is approximately

20 m wide and 26 m long, with the majority of the structure composed of 2 m × 2 m concrete bricks. In addition to two living buildings of roughly 5 m and 3 m in height to the west and east, the environment is open, and vegetation is primarily situated on the North and West sides of the square. Figure 2 shows the sequence of measurement and the measurement locations.

Figure 1: Heat square

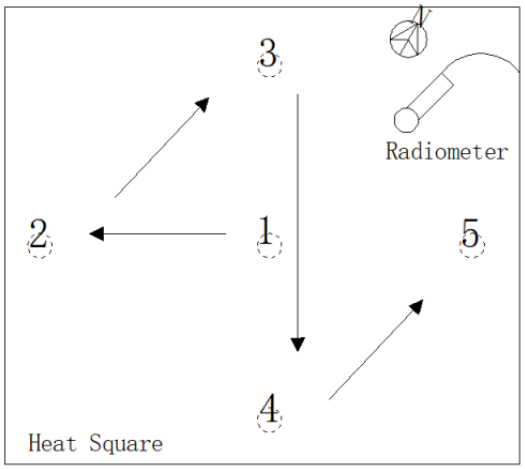

Figure 2: Location map

2.2 Equipment of measurements

The figure below shows the measurement equipment: Testo 174H(Figure 2.2) was used to measure air and ground temperatures, Testo 176T4(Figure 4) was used to measure the surface and bottom temperatures of concrete brick, and the radiometer(Figure 5) was used to monitor long and short wave radiation as well as the albedo.

Figure 3: Testo 174H for Air Temperature

Figure 4: Testo 176T4 for Surface and Bottom Temperature of Concrete

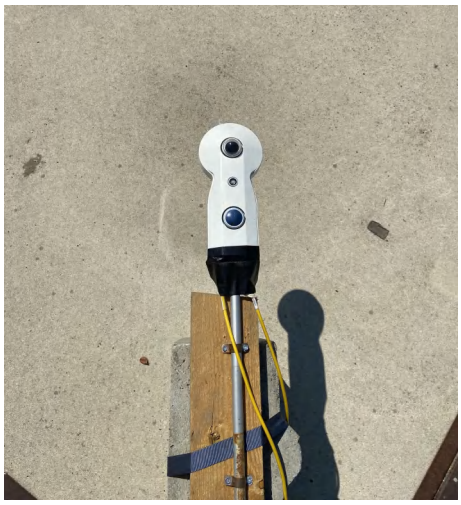

Figure 5: Radiometer

2.3 Description of Field Measurement

From July 18 to August 6, 2022, The devices were set up outside for 24 hours in sunny conditions (without cloud or precipitation). The measurement devices were distributed over five measurement locations in the Heat Square, with the locations changing every 24 hours on average. Temperature, humidity, radiation, and albedo are among the parameters measured in the experiment.

The temperature and humidity were first recorded at two-minute intervals on the surface and at a level of 1.4 m above the ground on a tripod with the Testo 174H. The temperature difference between the surface and 14 cm deep (slightly above soil) was measured with two measuring lines

set at two-minute intervals on the Testo 176T4. During the experiment, the 174H and 176T4 were covered with PVC material to avoid short-circuiting due to precipitation. The data was read out using Testo's Comsoft.

During the experiment, the radiometer did not change position with time and was placed in a north-south direction with a time zone offset of 1 hour. The temporal resolution of radiometer was one minute. The radiometer was read by a PC400 to obtain the short wave upper, short wave lower, long wave upper, long wave lower, and albedo, which were derived in the following analysis.

The Green Village measurement platform(Co-creation center, Figure 9) was also utilized to collect meteorological data for comparison purposes, such as illumination, wind speed, and temperature. The location of the sensor is on the roof of the building on the west side of Heat Square.

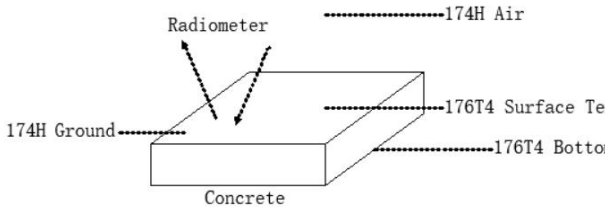

Figure 6: Equipment installation location

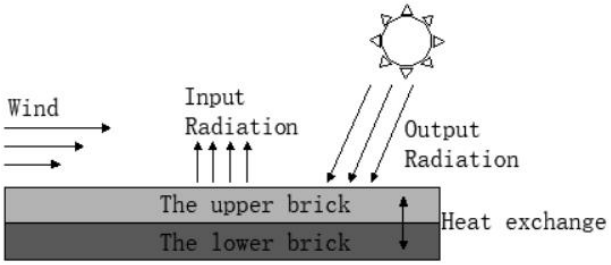

Figure 7: Heat budget

Figure 8: Field measurements

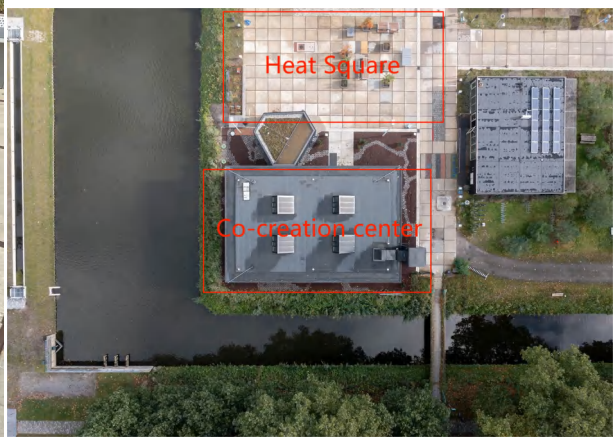

Figure 9: Location of Co-creation center

2.4 Ground heat flux

There are three fundamental methods for transferring heat energy: conduction, convection, and radiation. Heat conduction is the transfer of heat energy through the thermal movement of particles such as molecules and atoms of a substance when there is a temperature difference between two objects or when two objects of different temperatures come into contact with each other. Energy is exchanged when there is a temperature gradient within a substance. The one-dimensional conduction flux is defined as:

$$Q_{ground} = -\lambda \frac{\partial T}{\partial z} \tag{1}$$

where Q is the ground heat flux, defined as the amount of heat energy transported per unit time through a unit area of concrete block (W/m^2).$\partial T/\partial z$ represents the rate of change of temperature along the direction of temperature transfer, i.e., the derivative in the z-direction. λ is the thermal conductivity $[W/(m * k)]$, which reflects the magnitude of the material's ability to conduct heat, and the negative in the equation indicates that the direction of heat transfer is opposite to the direction of temperature increase. The value of λ for dense concrete brick is considered as 1.31 $W/(m{\cdot}K)$(*EngineeringToolBox*,2003).

2.5 Stefan-Boltzmann law

The measured upward long wave radiation can be verified by the Stephan-Boltzmann law.

$$L\uparrow = \varepsilon \sigma T^4 \tag{2}$$

where T is temperature(K). σ is the Stephan-Boltzmann constant with a value of 5.67×10^{-8} $W/(m^2 \times K^4)$. ε is emissivity of the object (blackness). In the case of an absolute blackbody, the ε=1. $L\uparrow$ is the long wave radiation (W).

2.6 Partial correlation analysis

Since the local climate environment is a multi-factor system with varied correlations between the various elements, the accuracy of assessing the correlation between surface temperature and a specific variable is usually affected by the interference of other factors. After this, partial correlation analysis was utilized to evaluate the relationship between surface temperature x and a specific variable y while controlling for other factors z. Hence, the partial correlation coefficient $r_{xy,z}$ is defined as:

$$r_{xy,z} = \frac{r_{xy} - r_{xz} \times r_{yz}}{\sqrt{(1 - r_{xz}^2) \times (1 - r_{yz}^2)}} \tag{3}$$

where r_{xy}, r_{xz}, r_{yz} are the correlation coefficients of the variables x and y, x and z, and y and z, respectively.

Partially correlation analysis was used in this study to evaluate the contribution of meteorological data such as wind speed, air temperature, and relative humidity to surface temperature. Since these data influence each other and the surface temperature, partial correlation analysis was chosen to analyze the contribution of a specific data set to the surface temperature by excluding the influence of other data.

2.7 Software

2.7.1 Testo ComSoft Basic 5.6

Comsoft Basic 5.6 is free software from Testo. Comsoft allows the programming and reading of Testo data loggers and has functions such as drawing graphs and tables and exporting.

2.7.2 SPSS 23

The widely used software for statistical data analysis is IBM SPSS Statistics 23. It includes functions for editing data, creating and editing graphs, and creating and editing tables. To obtain Pearson and partial correlation coefficients, a partial correlation analysis will be performed using SPSS on a combination of surface temperature and other meteorological data in this study.

2.7.3 Origin 2021

Origin 2021 is a scientific graphing and data analysis software program developed by OriginLab for use with Microsoft Windows. Origin is compatible with a wide range of 2D and 3D graphics. Statistics, signal processing, curve fitting, and peak analysis are all data analysis features in Origin.

3 Results

3.1 Temperature and Relative Humidity

The Figure 10 shows the temperature and humidity variations in heat square during the study period in sunny weather. The pattern of temperature and humidity variation during the day was derived by computing the hour-by-hour mathematical average of meteorological data over a 24-hour period. The variation in temperature and humidity follows a sinusoidal pattern, with the ground temperature generally higher than the air temperature over a 24-hour period, with the air and ground temperatures being closest at 9 a.m. during the day and the daily temperature difference reaching its maximum at 4 p.m. at approximately 6 °C. The daily maximum temperature is around 4 p.m., and the daily minimum temperature is around 6 a.m., so it takes 10 hours to rise from the minimum to the maximum, and 14 hours to fall from the maximum to the minimum, with certain temperature asymmetry. The slope of the curve is greatest between 8 a.m. and 10 a.m., showing

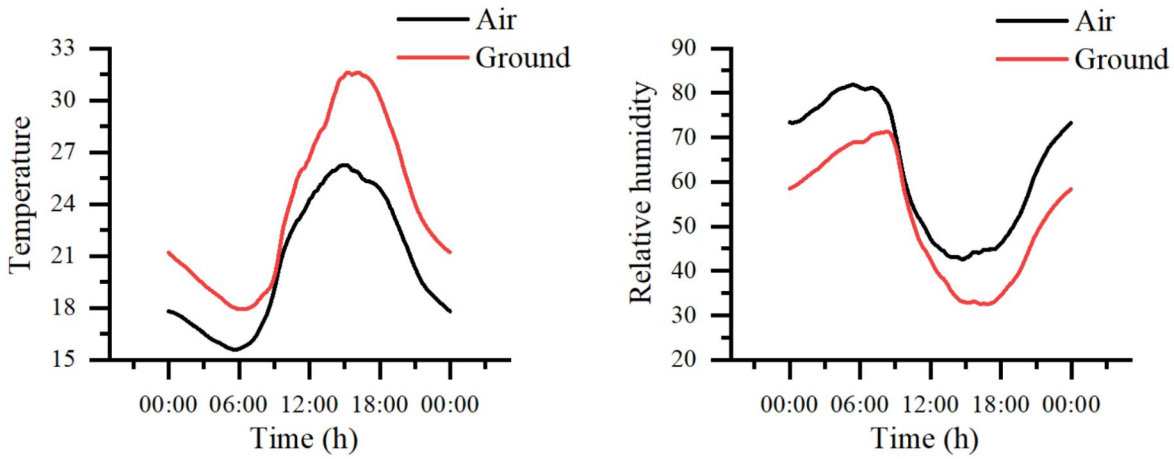

Figure 10: Trends in temperature(left) and humidity(right)

that the temperature rises fastest two hours after sunrise and similarly decreases fastest at 6 p.m., an hour before nightfall.

Changes in relative humidity follow a similar pattern, with relative humidity peaking immediately before sunrise and falling around sunset. At 8 *a.m.*, the air and surface relative humidity are at their lowest. The difference in relative humidity between the air and the surface is the largest around 4 p.m. and 6 a.m., at 10%.

3.2 Wind speed

Wind speed is a significant influence on surface temperature; its magnitude is directly related to air convection near the surface. The higher the wind speed, the faster the cooling rate near the surface. The wind speed data was collected at 10 minutes intervals from the green village monitoring platform, and the measured average wind speed data at each point is shown in the Figure 11. The variation in wind speed is less regular than the change in temperature, with wind speeds ranging from 0.1 m/s to 1 m/s. The average wind speed was 0.65 m/s throughout the day, with the largest wind speed reaching 6pm. The first order derivative of the surface temperature is shown in the Figure 12 and is defined in the analysis as the cooling rate. It can be seen from the Figure 12 that the cooling rate reaches a maximum at the time when the wind speed reaches its maximum.

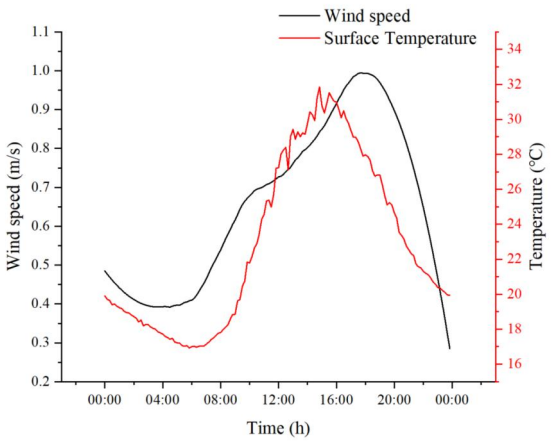

Figure 11: Trends in wind speed and surface temperature

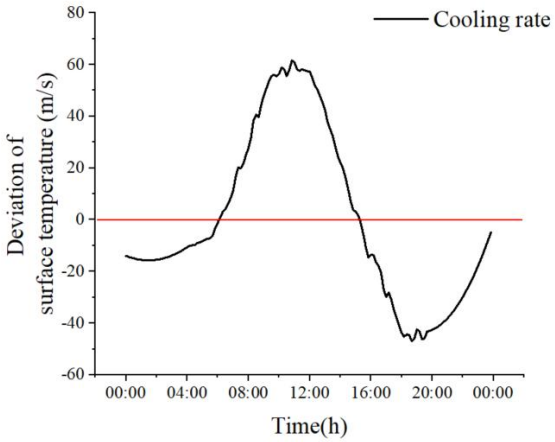

Figure 12: The deviation of surface temperature

3.3 Concrete temperature distribution

The Figure 13 shows the distribution of the daily average variation of the concrete brick's surface temperature and temperature at a depth of 14cm. The curve is similar to the temperature trend.

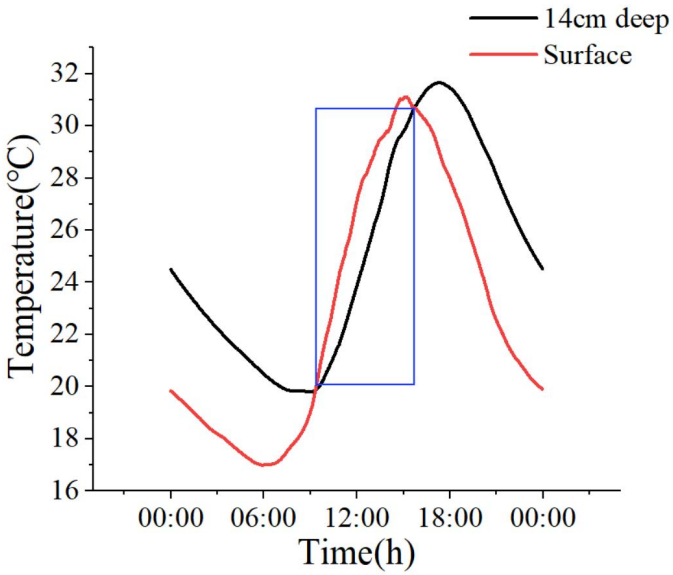

Figure 13: Temperature changes on the surface and bottom of concrete brick during the day

The blue line represents the time when the surface temperature is higher than the bottom temperature. The bottom temperature is higher than the surface temperature for the rest of the day. This demonstrates that heat is transmitted from the bottom upwards during periods of indirect sunlight, with a maximum temperature differential of 4 °C.

The surface temperature of the concrete fluctuates throughout the day, first declining, then increasing, and then decreasing again. The time period represented in the diagram is from 9 a.m. to 4 p.m., with the warming process lasting 7 hours and the cooling process lasting 17 hours, with the rate of warming much higher than the rate of cooling. The surface temperature of concrete

bricks delays with increasing depth, with the surface temperature peaking at 3 p.m. before the bottom temperature peaking at 6 p.m., showing a three-hour delay. The greatest temperature difference occurs not in the afternoon when solar energy is strongest, but in the early morning after sunset.

3.4 Precipitation period

The Figure 14 shows the temperature changes on the surface and bottom of concrete bricks caused by discontinuous precipitation events that occurred from 2022/7/20 to 2022/7/22. The precipitation resulted in an insignificant pattern of change between the surface and bottom of the variable concrete bricks. However, the surface temperature was always lower than the bottom temperature, with a temperature difference of approximately 2 °C. The reason for this was analyzed as evaporation of precipitation and the cooling effect resulting in a lower surface temperature.

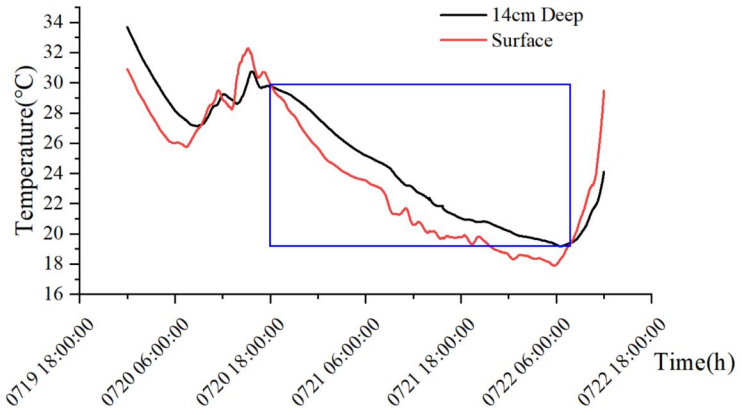

Figure 14: Temperature changes during the precipitation (19 July – 22 July).

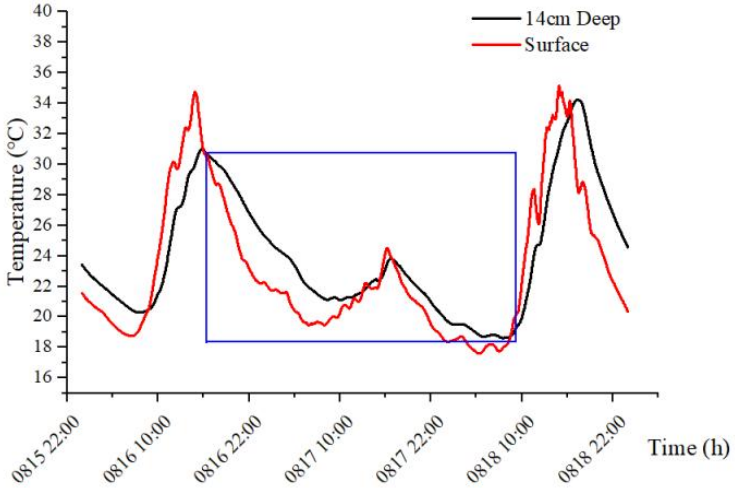

Figure 15: Temperature changes during the precipitation (15 August – 18 August).

The surface and bottom temperature changes for another rainfall event (15 August– 18 August) are shown in Figure 15. The rainfall in Figure 15 shows more similar results to the one in Figure 14.

3.5 Albedo and Radiation

The Figure 16 illustrates the 24-hour net radiation and also the hour-by-hour mean distribution of albedo. The net radiation distribution shows a normal distribution with a daily variation pattern, and the net radiation shows a single-peaked trend in terms of daily variation. The net radiation is

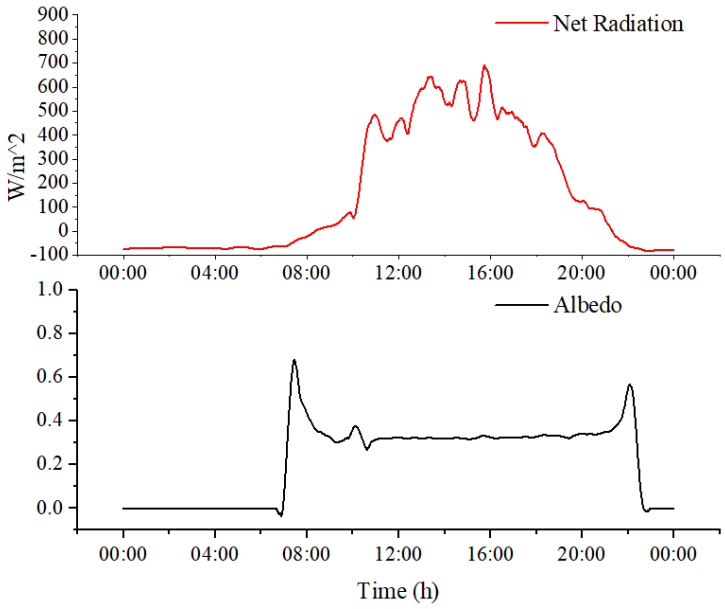

Figure 16: Net Radiation and Albedo

negative before sunrise and increases after sunrise as the solar altitude angle increases, reaching its maximum value for the day at 2pm–3pm, then decreasing until it becomes negative after sunset. Albedo fluctuates and peaks before and after sunrise, with a more moderate variation of about 0.31 during this period. Since the albedo is determined by the solar radiation and cannot be measured at night, its error increases at sunrise and sunset when the radiation varies widely, causing irregular albedo fluctuations at sunrise and sunset. Figure 17 shows the upward long-wave, downward long-wave, upward short-wave and downward short-wave radiation observed by the radiometer.

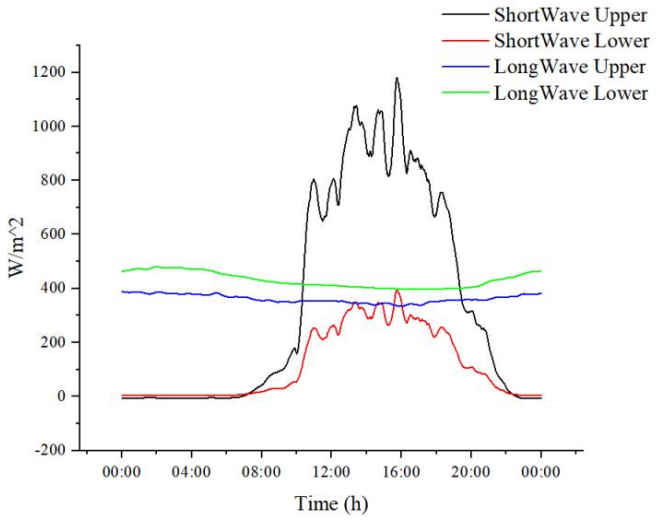

Figure 17: Long and Short Radiation

4 Discussion

4.1 Temperature

The net radiation peaks at the same time as the surface temperature, as demonstrated by the results above. At the same time, the lowest bottom temperature averages 25 °C throughout the day. Because of the lack of evaporation and the cooling effect of air convection, less heat is lost from the bottom of the concrete block, resulting in more heat being moved downwards and stored, prolonging the high temperature period and generating an asymmetry in the timing throughout the day. For the duration of the day, the average temperature differential between the bottom and surface temperatures is 2.2 °C. The surface of the concrete block warms up the fastest, followed by the bottom temperature, and finally the air temperature. Surface and air temperatures experienced similar valleys and peaks. It is worth noting that the surface and bottom of the concrete brick have similar maximum temperatures between the hours of 4 p.m. and 6 p.m., but during the trough between 6 a.m. and 9 a.m., the bottom temperature is approximately 4 °C higher than the surface temperature. At the same time, there is a three-hour lag between the lowest and highest temperatures. Such temperature change patterns verify the summer night-time warming effect of the local urban climate.

4.2 Partial correlation analysis

Table 1 presents the final results, which reveal that all significance levels were less than 0.05. With SPSS software, the surface temperatures were evaluated for a partial correlation with standardized wind speed, air temperature, relative humidity, net radiation, and illumination.

As can be seen from Table 1, changes in air temperature have the greatest effect on surface temperature, with a maximum partial correlation coefficient of 0.601. Changes in relative humidity have the lowest effect on surface temperature, with only 0.315. Wind speed and illumination have a negative partial correlation coefficient for surface temperature, but the Pearson coefficient is positive, indicating that wind speed and illumination contribute positively to surface temperature when combined with other factors, but negatively when other meteorological factors are excluded.

Table 1: The results of surface temperature partial correlation analysis

	Pearson coefficient	Partial correlation	degree of freedom
Wind speed	0.85	-0.321	138
Air Temperature	0.983	0.601	138
Relatively Humidity	-0.978	0.315	138
Net Radiation	0.933	0.379	138
Illumination	0.871	-0.524	138

The degree of freedom is defined as the number of independent variables that can be freely taken under certain constraints. The larger the degrees of freedom, the smaller the uncertainty and the more reliable the measurement results.

When the curves were further fitted by Origin (Figure 18), it was discovered that the R-squared was higher when fitting a polynomial relationship between surface temperature and wind speed, and that the values were closer to those in SPSS as the power increased. As a result, the relationship between surface temperature and wind speed can be approximated to be parabolic. This means that as the road surface temperature increases, the wind speed also increases, but after 26 °C, the wind speed tends to fluctuate as the road surface temperature increases.

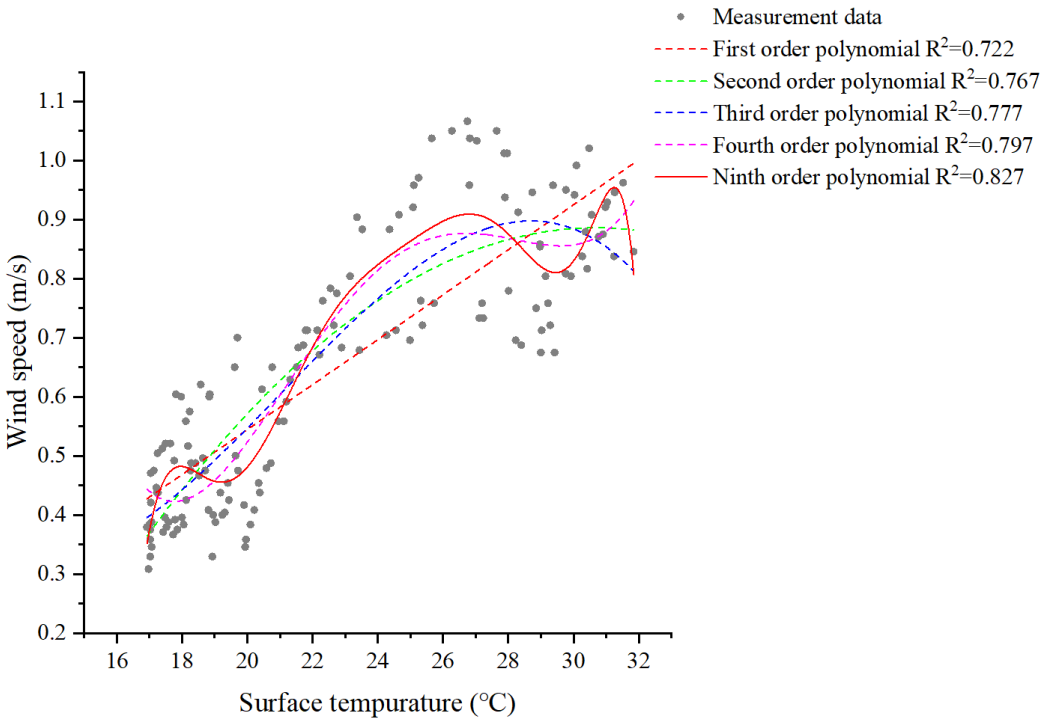

Figure 18: Polynomial fit of wind speed and surface temperature

4.3 Ground heat flux

The ground heat flux calculation is shown in Figure 19, and it is positive between 9 a.m. and 4

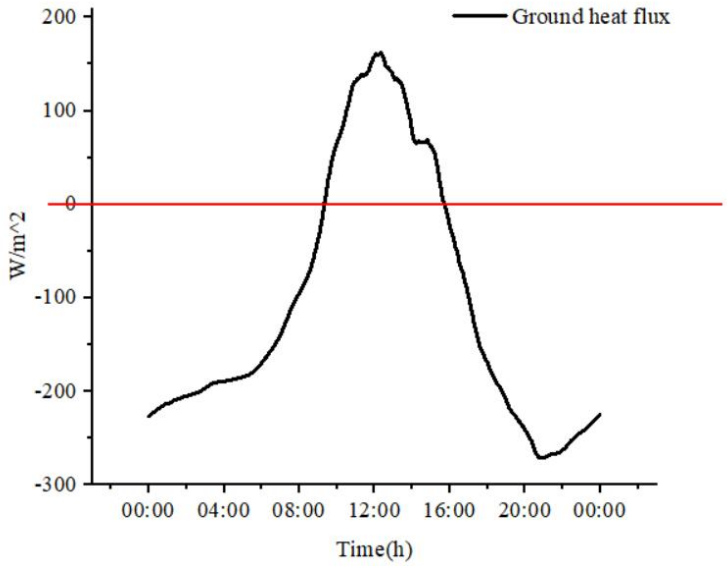

Figure 19: Ground heat flux

p.m., demonstrating a downward transfer of heat. The magnitude range is 10^1–10^2.

4.4 Stefan-Boltzmann law

The Figure 20 compares the results of the upward long wave radiation computed with Stephen Boltzmann's law to radiometer measurements. The figure illustrates that there is a 20–30% differ-

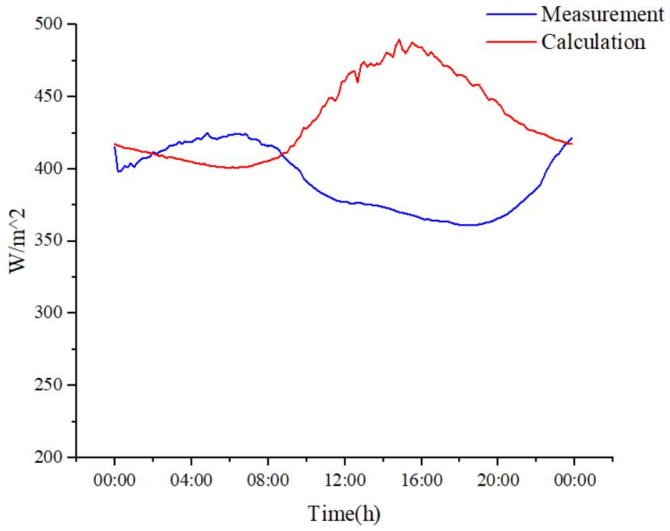

Figure 20: Comparison of calculated and measured values of long wave radiation

ence between the measured and calculated results during periods of high illumination, while the

data fits better for the rest of the period. In practice, the data could be corrected for periods of high sunlight intensity.

5 Suggestion

1. As the wind speed data in the study was obtained from the co-creation center in Green Village, which was placed at a height of 3 meters, it would be advisable to add near-ground wind speed measurements in later studies so that the correlation between surface temperature and wind speed can be better analyzed.

2. Temperature measurements are being added inside the brick at a depth of 5 cm, 10 cm from the ground. The temperature of the concrete brick pavement and top soil is measured by adding measurements at different depths, allowing temperature changes to be better analyzed.

3. The partial correlation coefficient for illumination is large in the partial correlation analysis, and subsequent studies can analyze the cooling effect under shaded conditions by studying the shading effect of plant shading.

6 Conclusion

Based on measurements collected over a month at the Green Village on the Delft campus, the paper explored the thermal behavior of the heat square in sunny summer conditions. The air and ground temperatures are closest during the day at 9 a.m., with a maximum daily temperature difference of around 6 °C at 4 p.m. The temperature increases most rapidly about two hours after sunrise and decreases most rapidly about one hour before sunset.

Throughout the day, the temperature of the concrete bricks changes asymmetrically, with the cooling time being much longer than the warming time. Second, the peaks and troughs of the surface and bottom temperatures have a three-hour time lag, even though the temperature difference between the peaks is only 0.5–1 °C, while the temperature difference between the valleys is 4 °C. The largest temperature difference occurs not in the afternoon, when solar radiation is greatest, but in the early morning hours after sunset. This also implies that one of the primary causes of the heat island effect is the thermal behavior of the concrete brick.

In the partial correlation analysis, the most significant influence of the meteorological factors (wind speed, air temperature, relative humidity, net radiation, illumination) on the surface temperature was the air temperature, with a maximum partial correlation coefficient of 0.601. The relative humidity variation had the least influence on the surface temperature, with only 0.315. By drawing a summary of the thermal behaviour of concrete brick pavements in the hot summer, it provides a basis for subsequent related studies. As well as a reference for urban construction, greening, etc.

References

Aletba, S. R. O., Abdul Hassan, N., Putra Jaya, R., Aminudin, E., Mahmud, M. Z. H., Mohamed, A., & Hussein, A. A. (2021). Thermal performance of cooling strategies for asphalt pavement: A state-of-the-art review. *Journal of Traffic and Transportation Engineering (English Edition)*, *8*(3), 356-373.

Anupam, B., Sahoo, U. C., & Rath, P. (2020). Phase change materials for pavement applications: A review. *Construction and Building Materials*, *247*, 118553.

Chudnovsky, A., Ben-Dor, E., & Saaroni, H. (2004). Diurnal thermal behavior of selected urban objects using remote sensing measurements. *Energy and Buildings*, *36*(11), 1063-1074.

Doulos, L., Santamouris, M., & Livada, I. (2004). Passive cooling of outdoor urban spaces. the role of materials. *Solar Energy*, *77*(2), 231-249.

Engineering ToolBox. (2003). Solids, liquids and gases - thermal conductivities. [online]. doi: https://www.engineeringtoolbox.com/thermal-conductivity-$d_4$29.*html*

Hove, B., Jacobs, C., Heusinkveld, B., Elbers, J., Driel, B., & Holtslag, B. (2014, 09). Temporal and spatial variability of urban heat island and thermal comfort within the rotterdam agglomeration. *Building and Environment*, *83*.

Middel, A., Turner, V. K., Schneider, F. A., Zhang, Y., & Stiller, M. (2020). Solar reflective pavements—a policy panacea to heat mitigation? *Environmental Research Letters*, *15*(6), 064016.

Stache, E. E., Schilperoort, B. B., Ottelé, M. M., & Jonkers, H. H. (2022). Comparative analysis in thermal behaviour of common urban building materials and vegetation and consequences for urban heat island effect. *Building and Environment*, *213*, 108489.

Wang, C., Wang, Z.-H., Kaloush, K. E., & Shacat, J. (2021). Cool pavements for urban heat island mitigation: A synthetic review. *Renewable and Sustainable Energy Reviews*, *146*, 111171.

Wonorahardjo, S., Sutjahja, I. M., Mardiyati, Y., Andoni, H., Achsani, R. A., Steven, S., ... Tedja, S. (2022). Effect of different building façade systems on thermal comfort and urban heat island phenomenon: An experimental analysis. *Building and Environment*, *217*, 109063.

Yang, X., & Zhao, L. (2016). Diurnal thermal behavior of pavements, vegetation, and water pond in a hot-humid city. *Buildings*, *6*(1). doi: 10.3390/buildings6010002